Journal of Zhejiang University SCIENCE A
ISSN 1009-3095 (Print); ISSN 1862-1775 (Online)
www.zju.edu.cn/jzus; www.springerlink.com
E-mail: jzus@zju.edu.cn

Bubble entrainment, spray and splashing at hydraulic jumps

CHANSON Hubert
(*Division of Civil Engineering, The University of Queensland, Brisbane QLD 4072, Australia*)
E-mail: h.chanson@uq.edu.au

Received Mar. 16, 2006; revision accepted Apr. 8, 2006

Abstract: The sudden transition from a high-velocity, supercritical open channel flow into a slow-moving sub-critical flow is a hydraulic jump. Such a flow is characterised by a sudden rise of the free-surface, with some strong energy dissipation and air entrainment, waves and spray. New two-phase flow measurements were performed in the developing flow region using a large-size facility operating at large Reynolds numbers. The experimental results demonstrated the complexity of the flow with a developing mixing layer in which entrained bubbles are advected in a high shear stress flow. The relationship between bubble count rates and void fractions was non-unique in the shear zone, supporting earlier observations of some form of double diffusion process between momentum and air bubbles. In the upper region, the flow consisted primarily of water drops and packets surrounded by air. Visually significant pray and splashing were significant above the jump roller. The present study is the first comprehensive study detailing the two-phase flow properties of both the bubbly and spray regions of hydraulic jumps, a first step towards understanding the interactions between bubble entrainment and droplet ejection processes.

Key words: Hydraulic jump, Air bubble entrainment, Spray and splashing physical modelling, Particle chord time distributions
doi:10.1631/jzus.2006.A1396 **Document code:** A **CLC number:** O359$^+$.1

INTRODUCTION

A hydraulic jump is the sudden transition from a high-velocity, supercritical open channel flow into a slow-moving, sub-critical flow (Belanger, 1840; Bakhmeteff, 1932; Henderson, 1966; Chanson, 2004a). It is characterised by a sudden rise of the free-surface, with some strong energy dissipation and mixing, large-scale turbulence, air entrainment, waves and spray (Fig.1). Early experimental studies of air bubble entrainment were conducted in terms of the quantity of entrained air primarily (Wisner, 1965; Rao and Kobus, 1971). Experimental studies of the bubbly flow's microscopic structure included Rajaratnam (1962) and Resch and Leutheusser (1972), and more recent advanced studies encompassed the works of (Mossa and Tolve, 1998; Chanson and Brattberg, 2000; Murzyn *et al*., 2005). Despite these pertinent studies, the interactions between air bubble entrainment, and spray and splashing are not yet completely understood.

In the present study, new air-water flow measurements were performed in hydraulic jumps. The experiments were performed in a relatively large-size facility with a fine phase-detection probe. It is the purpose of this study to document the air bubble entrainment process, as well as the spray and splashing above the roller.

Dimensional considerations

In the study of air bubble entrainment in hydraulic jumps, the relevant parameters for a dimensional analysis include the fluid properties and physical constants, the channel geometry and inflow conditions, and the air-water flow properties including the bubble and droplet characteristics. Considering the simple case of a hydraulic jump in a horizontal, rectangular channel, a dimensional analysis yields:

$$C, F, V, d_{ab}, d_{wd}, \ldots = F_1(x, y, z, d_1, V_1, x_1, \delta, W, k_s, g, \rho_{air}, \rho_w, \mu_{air}, \mu_w, \ldots), \quad (1)$$

where C is the void fraction, F is the bubble count rate, V is the velocity, d_{ab} is a characteristic size of

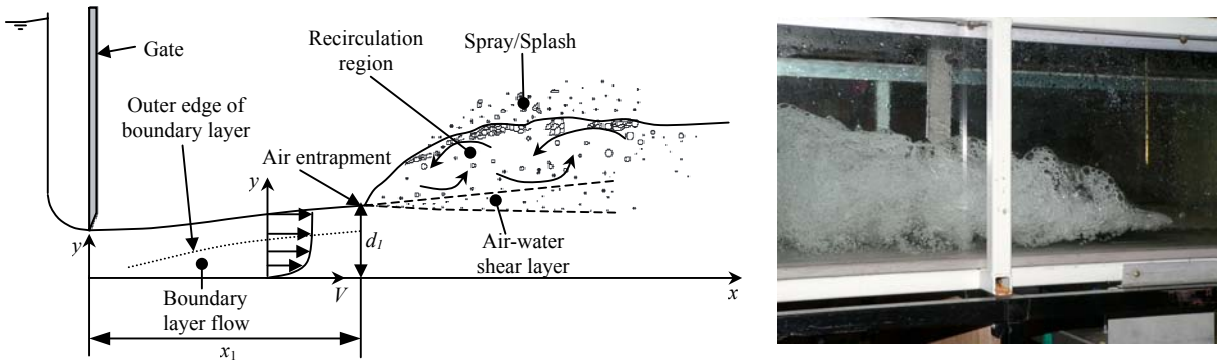

(a) (b)

Fig.1 Air bubble entrainment in a hydraulic jump. (a) Definition sketch of a hydraulic jump with partially-developed inflow condition; (b) High-shutter speed photograph (1/1000 s)

entrained bubble, d_{wd} is a characteristic size of water droplet, x is the coordinate in the flow direction measured from the nozzle, y is the vertical coordinate, z is the transverse coordinate measured from the channel centreline, d_1 is the inflow depth, V_1 is the inflow velocity, x_1 is the distance from the upstream gate (Fig.1a), δ is the boundary layer thickness of the inflow, W is the channel width, k_s is the bed roughness height, g is the gravity acceleration, ρ_w and μ_w are the water density and dynamic viscosity respectively, ρ_{air} and μ_{air} are the air density and dynamic viscosity respectively, σ is the surface tension between air and water.

Eq.(1) expresses the air-water flow properties (left hand side terms) at a position (x, y, z) as functions of the inflow properties, channel geometry and fluid properties. In addition, biochemical properties of the water solution might be considered. Compressibility of high-velocity air-water flow may also be an issue, although a re-analysis of existing model and prototype data with transonic and supersonic flow conditions showed little compressibility effects in free-surface flows (Chanson, 1997; 2004b). Herein compressibility effects are not considered here. Further, if the local void fraction is known, the density and viscosity of the air-water mixture can be deduced as $\rho_w \cdot (1-C)$ and $\mu_w \cdot (1+2.5C)$ respectively (Einstein, 1906; 1911), and the parameters ρ_{air} and μ_{air} may be ignored. A smooth, wide channel is also considered, and the effects of bed roughness and channel width are ignored in the first approximation.

Eq.(1) may be transformed into dimensionless terms:

$$C, \frac{Fd_1}{V_1}, \frac{V}{\sqrt{gd_1}}, \frac{d_{ab}}{d_1}, \frac{d_{wd}}{d_1}, \ldots = F_2\left(\frac{x-x_1}{d_1}, \frac{y}{d_1}, \frac{x_1}{d_1}, \frac{V_1}{\sqrt{gd_1}}, \rho_w \frac{V_1 d_1}{\mu_w}, \frac{\delta}{d_1}, \frac{W}{d_1}, \frac{g\mu_w^4}{\rho_w \sigma^3}, \ldots\right). \quad (2)$$

In the right hand side of Eq.(2), the fifth and sixth terms are the inflow Froude Fr_1 and Reynolds numbers Re_1 respectively. The seventh term is the Morton number Mo that is a function of fluid properties and gravity constant only.

Dynamic similarity

In open channel flows including hydraulic jumps, a Froude similitude is commonly used (Henderson, 1966; Chanson, 2004a). That is, the Froude number characterising the ratio of the inertial force to gravity force must be equal in both model and prototype. But the entrapment and advection of air bubbles, the mechanisms of air bubble breakup and coalescence, and water droplet ejections are affected by viscous and surface tension effects implying the need for a Reynolds similitude that cannot be satisfied in small size models. In other words, Eq.(2) demonstrates that the dynamic similarity of air bubble entrainment and droplet generation in hydraulic jumps is nearly impossible with geometrically similar models because of the too many relevant parameters.

Any combination of these dimensionless numbers is also dimensionless. That is, it may be used to replace one of the above combinations. For example, the Reynolds number could be replaced by the Weber

number $We_1=\rho_w V_1^2 d_1/\sigma$ or by the Eötvös number $Eo_1=\rho_w g d_1^2/\sigma$. The Weber number is proportional to the ratio of the inertial to capillary forces, while the Eötvös number is the ratio of a Weber number to a Froude number. Note that, for the same fluids (air and water) in both model and prototype, the Morton number *Mo* becomes a constant, and Eq.(2) may be slightly simplified.

EXPERIMENTAL SETUP

Presentation

New experiments were performed in a large-size free-surface water channel at the University of Queensland (Table 1). The channel was horizontal, 3.2 m long and 0.5 m wide (Fig.1b). The sidewalls were made of 3.2 m long glass panels and the bed was made of 12 mm thick PVC sheets. The inflow was controlled by a rounded gate and the downstream coefficient of contraction was about unity. Upstream of the gate, the flow from a large reservoir passed through a system of screens and flow straighteners to ensure a quiescent and two-dimensional flow into the head tank immediately upstream of the gate. This arrangement generated in turn a well-defined shallow supercritical approach flow downstream of the gate.

Table 1 Summary of experimental flow conditions

d_1 (m)	x_1 (m)	V_1 (m/s)	Fr_1	Re_1	$x-x_1$ (m)	Comments
0.0265	1.0	2.6	5.1	6.8×10^4	0.1 0.2 0.3	Run 051202
0.0238	1.0	4.14	8.6	9.8×10^4	0.1 0.2 0.4	Run 051206

Note: x_1 is the distance between the upstream gate and jump toe; $Fr_1=V_1/\sqrt{gd_1}$; $Re_1=\rho_w V_1 d_1/\mu_w$

The waters were supplied by a constant head system. The water discharge was measured with a Venturi meter which was calibrated in-situ with a large V-notch weir. The percentage of error was expected to be less than 2%. The water depths were measured using rail mounted pointer gauges with an accuracy of 0.2 mm. Preliminary clear water velocity measurements were performed using a Prandtl-Pitot tube (3.3 mm external diameter). These results showed that the supercritical inflow was partially-developed for all investigated flow conditions listed in Table 1.

Air-water flow properties were measured with a single-tip conductivity probe based upon a needle probe design. The probe sensor consisted of a sharpened rod (Φ=0.35 mm) which was insulated except for its tip and set into a metal supporting tube (Φ=1.42 mm) acting as the second electrode. The probe was excited by an electronics device designed with a response time less than 10 μs. The probe sensor was scanned at 20 kHz for 45 s. All measurements were conducted on the channel centerline. Note that phase-detection probes such as the conductivity probe are very sensitive devices susceptible to a number of problems. In the present study, the probe signals were checked systematically for long-term signal decays induced by probe tip contamination, short-term signal fluctuations caused by debris and water impurities, electrical noise and spurious samples. While some quality control procedure can be computerised, it must be stressed that human supervision and intervention are essential to validate each quality control step.

Further information on the experiments and on the instrumentation were detailed in (Chanson, 2006).

Signal processing and data analysis

The measurement principle of a conductivity probe is based upon the difference in electrical resistivity between air and water (Crowe *et al*., 1998; Chanson, 1997; 2002). In the present study, the air-water flow properties were calculated using a single threshold technique, with the threshold set at about 45%~55% of the air-water voltage range.

The void fraction *C* is the proportion of time that the probe tip is in the air. The bubble count rate *F* is the number of bubbles/droplets impacting the probe sensor per second. The measurement is sensitive to the probe tip size, bubble sizes, velocity and discrimination technique, particularly when the sensor size is larger than the smallest particles. The bubble/droplet chord time is defined as the time spent by the bubble/droplet on the probe tip. Bubble/droplet chord times were calculated from the raw probe signal using the single threshold method. Statistical analyses of chord time distributions yielded the median value and the statistical moments of both air and water chord times, as well as the streamwise structure of the air-water flow.

BASIC AIR-WATER FLOW PROPERTIES

A hydraulic jump flow is characterised by the development of large-scale turbulence. At the jump toe, air packets are entrained into a developing shear layer characterised by intensive turbulence production (Fig.1). Air can be entrained by a combination of different mechanisms. If the inflow is aerated upstream of the intersection with the pool of water, the aerated layer at the jet free-surface is entrained past the impingement point. This process is also called pre-entrainment or two-phase flow air flux (Thandaveswara, 1974). Further, an air layer is set into motion by shear friction next to the free-surface of the impinging flow and some air is trapped at the entrainment point. Another mechanism is the aspiration of the induction trumpet formed at the intersection of the water jet with the roller (i.e. jump toe). At the closure of the trumpet, air packets are entrapped and entrained within the shear flow (Chanson and Brattberg, 1998).

Downstream of the jump toe, the entrained air packets are broken up into small bubbles as they are advected in the shear region (Fig.1). Once the entrained bubbles are advected into regions of lesser shear, bubble collisions and coalescence become predominant, leading to larger air entities (bubbles, pockets) that are driven towards the free-surface by buoyancy. In the recirculating region, strong unsteady flow reversal and recirculation occur. The location of the jump toe consistently fluctuated around its mean position and some "vortex shedding" developed in the mixing layer. High-speed photographs showed a significant number of air-water ejections above the mean "free-surface" of the roller (Fig.1b). The ejected packets re-attached rapidly to the jump roller and are not always seen by eye. The bulk of the roller is further enhanced by the volume of the entrained air. Visual observations suggested that the maximum roller height was about 10%~20% larger than the downstream flow depth (i.e. conjugate depth) depending upon the inflow Froude numbers and experimental conditions.

Typical observations of void fractions and bubble count rate distributions are presented in Fig.2. The void fraction distributions exhibited a peak in the turbulent shear region that was previously observed in hydraulic jumps with partially-developed inflow (Chanson and Brattberg, 2000; Murzyn *et al*., 2005). The peak void fraction C_{max} decreased with increasing distance ($x-x_1$) from the jump toe while this air advection/diffusion layer broadened. Similarly a maximum F_{max} in the bubble count rate was observed in the developing mixing region although its location did not coincide with the location of maximum void fraction. It was suggested that the non-coincidence illustrated a double diffusion process whereby air bubbles and momentum diffused at different rates and in a different manner (Chanson and Brattberg, 2000). Indeed, the interactions between developing shear layer and air advection layer are complicated and not yet well understood.

In the air advection layer, the void fraction distributions followed closely an analytical solution of the advective diffusion equation for air bubbles:

$$C = C_{max} \cdot \exp\left[-\frac{1}{4D^{\#}} \cdot \frac{\left(\frac{y}{d_1} - \frac{Y_{C_{max}}}{d_1} \right)^2}{\frac{x - x_1}{d_1}} \right]$$

Air advection/diffusion layer, (3)

where C_{max} is the maximum air content in the turbulent shear layer region observed at $y = Y_{C_{max}}$, x and y are the longitudinal and vertical distances measured from the channel intake and bed respectively, and x_1 is the location of the jump toe, $D^{\#}$ is a dimensionless diffusivity: $D^{\#} = D_t/(V_1 d_1)$, D_t is the turbulent diffusivity which averages the effects of turbulent diffusion and of longitudinal velocity gradient, V_1 is the inflow velocity, and d_1 is the inflow depth (Chanson, 1997). Eq.(3) is compared with experimental data in Fig.2a. Values of $D^{\#}$ were estimated from the best data fit. In the present study, Eq.(3) was observed in the developing flow region. Further downstream, the advection layer broadened and air detrainment destroyed the organised mixing layer (Herein air detrainment defines an upward advection of air bubbles towards the free-surface and the atmosphere, typically induced by buoyancy).

In the upper region of the roller, the void fraction distributions tended to follow a solution of the bubble advection equation for a free-jet:

$$C = \frac{1}{2}\left[1 + erf\left(\frac{1}{2}\sqrt{\frac{V_1}{D_t'}} \frac{y - Y_{50}}{\sqrt{x - x_1}} \right) \right]$$

Upper free-surface, (4)

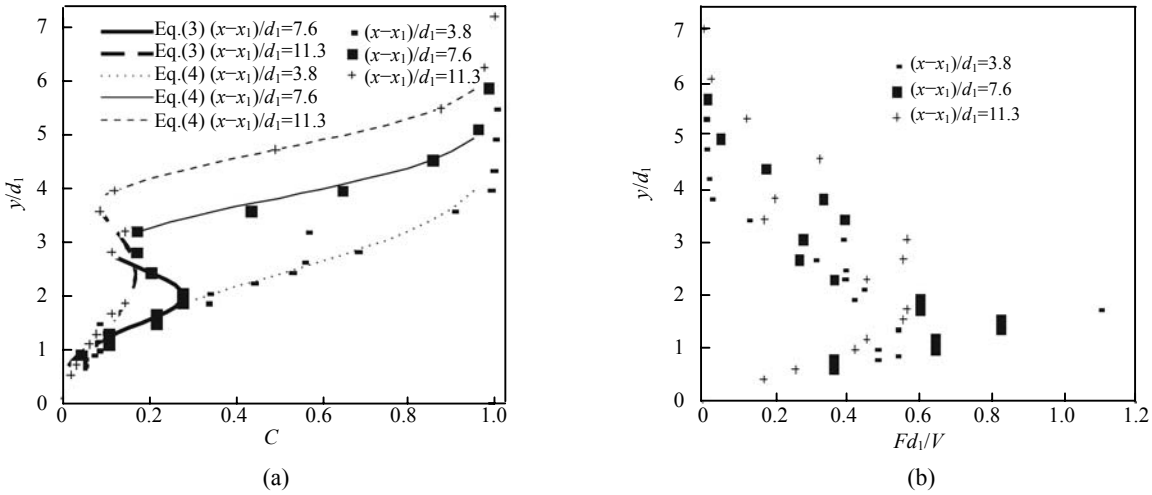

Fig.2 Dimensionless distributions of void fractions and bubble count rate in the developing flow region. Fr_1=5.1, d_1=0.0265 m, x_1=1 m, $x-x_1$=0.1, 0.2 and 0.3 m. (a) Void fraction distributions: comparison with Eqs.(3) and (4); (b) Dimensionless bubble count rate distributions

where Y_{50} is the characteristic depth (m) where the void fraction is 50%, D'_t is the turbulent diffusivity of the upper interface and *erf*() is the Gaussian error function:

$$erf(u)=\frac{2}{\sqrt{\pi}}\int_0^u \exp(-t^2)\mathrm{d}t \,. \tag{5}$$

Eq.(4) was first derived by Chanson (1989) for water jets discharging into air with uniform velocity distribution, for a diffusivity D'_t that is assumed independent of the transverse direction y and which averages the effect of turbulence and longitudinal velocity gradient (Chanson, 1997; Brattberg *et al*., 1998). Note that D'_t characterises the air bubble diffusion process at the upper free-surface while, in Eq.(3), the diffusivity D_t describes the advective diffusion process in the air-water shear layer downstream of a point source at $x=x_1$ and $y=d_1$ (i.e. jump toe). Strictly speaking, Eq.(4) is not applicable to a hydraulic jump roller "free-surface", although it does fit the data (Murzyn *et al*., 2005; the present study). It is shown in Fig.2a for completeness.

Relationship between void fraction and bubble count rate

Typical bubble count rate distributions are presented in Fig.2b. At each cross-section, the bubble count rate distribution exhibited a characteristic maximum in the mixing layer. However it may also be presented as a function of the void fraction (Fig.3). The experimental data in the mixing layer suggested that the relationship between bubble frequency and void fraction was not unique. For $y< Y_{C_{max}}$, the bubble count rate was always larger, for a given void fraction, than for $y> Y_{C_{max}}$ (Fig.3). Fig.3 illustrates some experimental results.

A similar finding was obtained in the advective diffusion region of vertical plunging jets (Brattberg *et al*., 1998), although it had not been documented in hydraulic jumps. The present finding is limited to the developing flow region of the advective diffusion zone. This form of hysteresis between F and C must be related to some dissymmetry in the momentum mixing layer including the position of maximum shear stress, and possibly the local state of shear. For a given void fraction, the bubble count rate is larger in regions of high shear and large velocity, which may also be related to some form of interactions between entrained bubbles and turbulent structures. These interactions are likely responsible for the double diffusion process whereas air bubbles and momentum diffuse at a different rate and in a different manner in the mixing layer as documented by the data of (Resch and Leutheusser, 1972; Chanson and Brattberg, 2000).

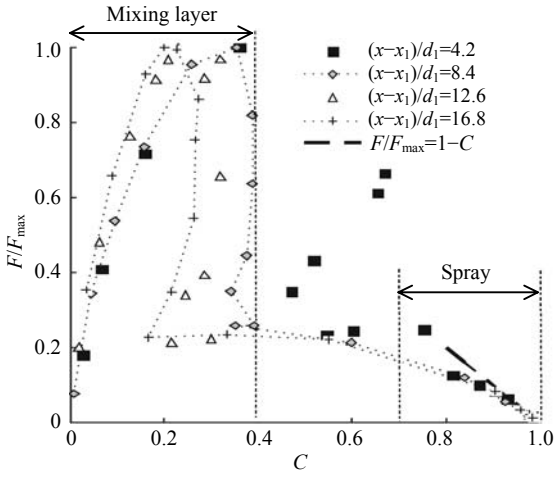

Fig.3 Dimensionless relationship between void fraction and bubble count rate in the developing flow region. Fr_1=8.6, d_1=0.024 m, x_1=1 m, $x-x_1$=0.1, 0.2, 0.3 and 0.4 m, compared with Eq.(6)

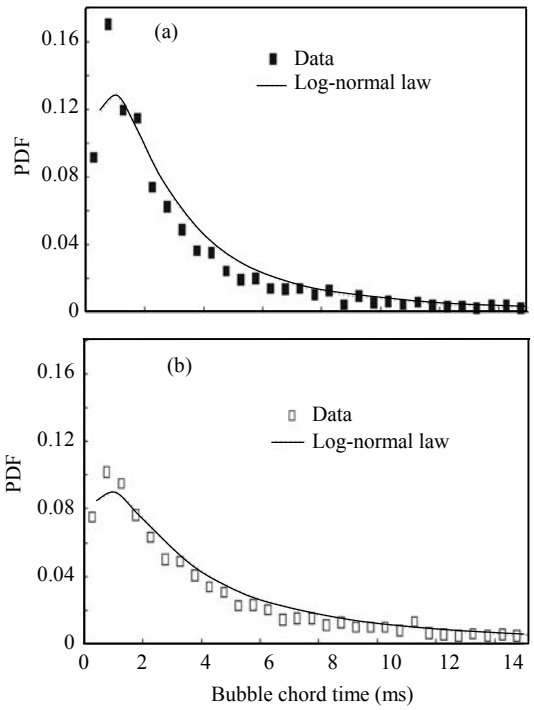

Fig.4 Bubble chord time distributions in the bubbly flow region at the location of maximum buble count rate (F=F_{max}), PDF with 0.5 ms chord time intervals. (a) Fr_1=5.1, d_1=0.0265 m, x_1=1 m, $x-x_1$=0.2 m, y=0.0365 m, C=0.218, F=80.9 Hz, Nb=3641, median air chord time is 1.35 ms, standard deviation is 4.09 ms, skewness is 4.38, excess kurtosis is 28.6; (b) Fr_1=8.6, d_1=0.024 m, x_1=1 m, $x-x_1$=0.2 m, y=0.03165 m, C=0.353, F=186.3 Hz, Nb=8000, median air chord time is 0.70 ms, standard deviation is 25.7 ms, skewness is 87.8, excess kurtosis is 7803

BUBBLE CHORD TIME DISTRIBUTIONS

Air chord times in the developing shear layer were recorded. The bubble chord time is proportional to the bubble chord length and inversely proportional to the velocity. In a complicated flow such as a hydraulic jump where flow reversal and recirculation exist, phase-detection intrusive probe cannot discriminate accurately the direction or magnitude of the velocity. Most single- and dual-tip probes are designed to measure positive velocities only and the probe sensor would be affected by wake effects during flow reversal. Therefore only air/water chord times are genuine data. Note that air/water chord times are shown in ms. For a 1 m/s particle velocity, a 1 ms chord time would correspond to a 1 mm particle chord length.

Fig.4 shows typical normalised bubble chord time distributions for two inflow Froude numbers. Each dataset was obtained at the location of maximum bubble count rate F_{max} at the same dimensionless distance from the jump toe $(x-x_1)/d_1$=8. For Figs.4a and 4b, the legend provides the inflow conditions, physical location, local air-water flow properties (C, F), number of recorded bubbles and the statistics of the bubble chord times. On the graph, each data point represents the probability of bubble chord time in a 0.5 ms chord time interval. For example, the probability of bubble chord time from 1 to 1.5 ms is represented by the data point labelled 1.25 ms. For conciseness bubble chord times larger than 15 ms are not shown.

Overall, the results highlighted a broad spectrum of bubble chord times at each location. The range of bubble chord time extended over several orders of magnitude, including at low void fractions, from less than 0.1 ms to more than 15 ms. Small bubble chord times corresponded to small bubbles passing rapidly in front the probe sensor, and large chord times implied large air packets flowing slowly past the probe sensor. For intermediate chord times, there was a wide range of possibilities in terms of bubble sizes depending upon the bubble velocity.

Furthermore the distributions were skewed with a preponderance of small bubble chord time relative to the mean. In Fig.4a, the probability of bubble chord

time is the largest for chord times between 0.5 and 1 ms. In Fig.4b, the mode is about 0.5~1.5 ms owing to larger velocities at higher Froude and Reynolds numbers than for the flow conditions corresponding to Fig.4a. The probability distribution functions of bubble chord time tended to follow log-normal distribution. An example of comparison between data and log-normal distribution is shown in Fig.4.

Moreover the air chord time distributions had similar shape at most vertical locations although the air-water structures appeared to differ across the mixing layer.

SPRAY AND SPLASHING ABOVE THE HYDRAULIC JUMP ROLLER

The study of spray and splashing is limited to high-velocity water flows. Some researchers used visual techniques while others used intrusive phase detection probes (Chanson, 1999; Toombes, 2002; Hong *et al*., 2004). Observations on highly turbulent open channel flows suggested that the upper air-water flow region with void fractions greater than 0.70 consists primarily of water structures surrounded by air: i.e., the spray region. However such a spray region defined as $C>0.7$ may comprise several sub-layers: (1) a spray/splashing region consisting of relatively large water droplets, packets and entities surrounded by air for $0.7<C<0.9$, (2) a spray/mist region with smaller densities of water droplets for $0.9<C<0.99$, and (3) an upper fog/aerosol region with very-fine water droplets (Toombes, 2002; Chanson and Gonzalez, 2004). In the spray region, drop formation results from surface distortion, tip-streaming of ligaments and interactions between eddies and free-surface (Hoyt and Taylor, 1977; Rein, 1998). The formation and ejection of a droplet must be associated with a transfer of turbulent kinetic energy from the main flow. Once a droplet is ejected, its ejection process is the dominant effect because the droplet response time is nearly two orders of magnitude larger than the airflow response time. The energy of each droplet is a combination of its potential energy and kinetic energy.

During the present study, visual observations showed a substantial amount of air-water projections and splashing above the roller, particularly at the largest Reynolds number. Most ejected structures were water and water-and-air packets surrounded by air (Fig.5). Fig.5 presents some high-shutter speed photographs of the upper flow region above the hydraulic jump roller showing instantaneous water spray structures. Note the variety of instantaneous water entity shapes. Visually the spray region appeared to be very similar to that observed in open channel flow with a spray/mist and fog/aerosol region in the upper layers.

Detailed water chord time measurements were conducted in the upper flow layers. Figs.6 and 7 show typical droplet chord time distributions at various vertical elevations above the jump roller for both inflow Froude numbers. For each figure, the caption provides the local air-water flow properties (C, F) and the number of recorded droplets during the scan period (t=45 s). The histogram columns each represent the probability of droplet chord time in a 0.5 ms interval. Drop chord times larger than 15 ms are regrouped in the last column (>15).

First, note the broad spectrum of droplet chord time at each location (Figs.6 and 7). The range of drop chord times extends over several orders of magnitude

(a) (b) (c)

Fig.5 High-shutter photographs of instantaneous spray/splash structures. Fr_1=8.6, d_1=0.024 m, V_1=4.1 m/s, x_1=1 m, flow from right to left (shutter 1/1000 s). (a) Side view of the roller; (b) Details of some instantaneous air-water projections; (c) Details of the instantaneous roller free-surface

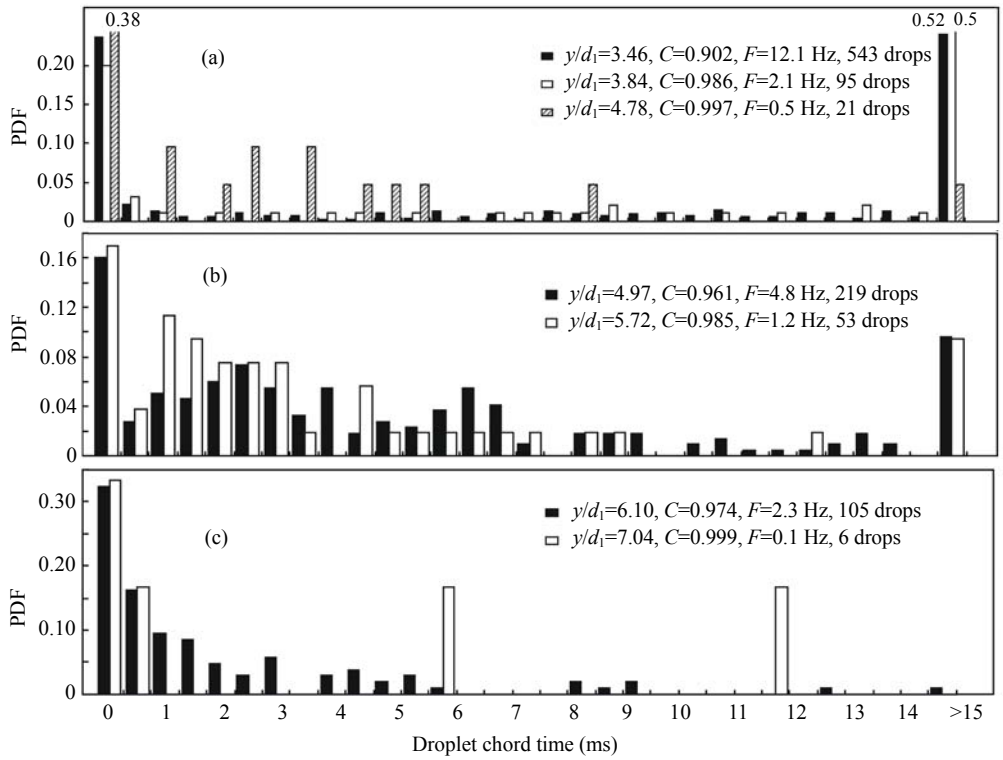

Fig.6 Drop chord time distributions in the spray/mist region. Fr_1=5.1, Re_1=6.8×10^4, d_1=0.0265 m, x_1=1.0 m, W=0.50 m. (a) $x-x_1$=0.1 m; (b) $x-x_1$=0.2 m; (c) $x-x_1$=0.3 m

from less than 0.5 ms to more than 15 ms. Such a range would correspond to tiny droplets flowing at high velocity to large water packets moving at low speed past the probe.

Second, the water drop chord time distributions did not exhibit a shape similar to air chord time distributions that were observed in the bubbly flow region of the hydraulic jump flow. A comparison between Fig.4 and Figs.6 and 7 shows broader water chord time PDFs in the spray/mist region and upper fog/aerosol region. Such a type of flat, uneven distributions are undocumented up to date.

Third, the number of droplets was small at low liquid fractions implying that longer scan durations are required to gain a better description of the spray/mist statistical properties. Despite limited number of detected droplets, the relationship between droplet count rate F and liquid fraction $(1-C)$ is as follows:

$$F/F_{max}\approx 1-C \quad (6)$$

in the upper fog/aerosol region. Eq.(6) is shown in Fig.3.

SUMMARY AND CONCLUSION

New two-phase flow measurements were performed in the developing flow region of hydraulic jumps. The experiments were conducted in a large-size facility operating at large Reynolds numbers to minimise scale effects that may be associated with the extrapolation of the results to typical civil and environmental engineering applications.

The experimental results demonstrated the complexity of the flow with a developing mixing layer in which entrained bubbles are advected while they are subjected to high shear stress. In the shear layer region, the void fraction distributions followed closely an analytical solution (Eq.(3)) of the advection diffusion equation for air bubbles downstream of a point source (i.e. the entrapment point). The relationship between bubble count rates and void fractions was not unique in the shear zone, supporting earlier observations of a double diffusion process whereby momentum and air bubbles diffuse in a different manner and at a different rate. The distributions of bubble chord times showed a wide range of measured chord times, which followed closely a log-normal profile.

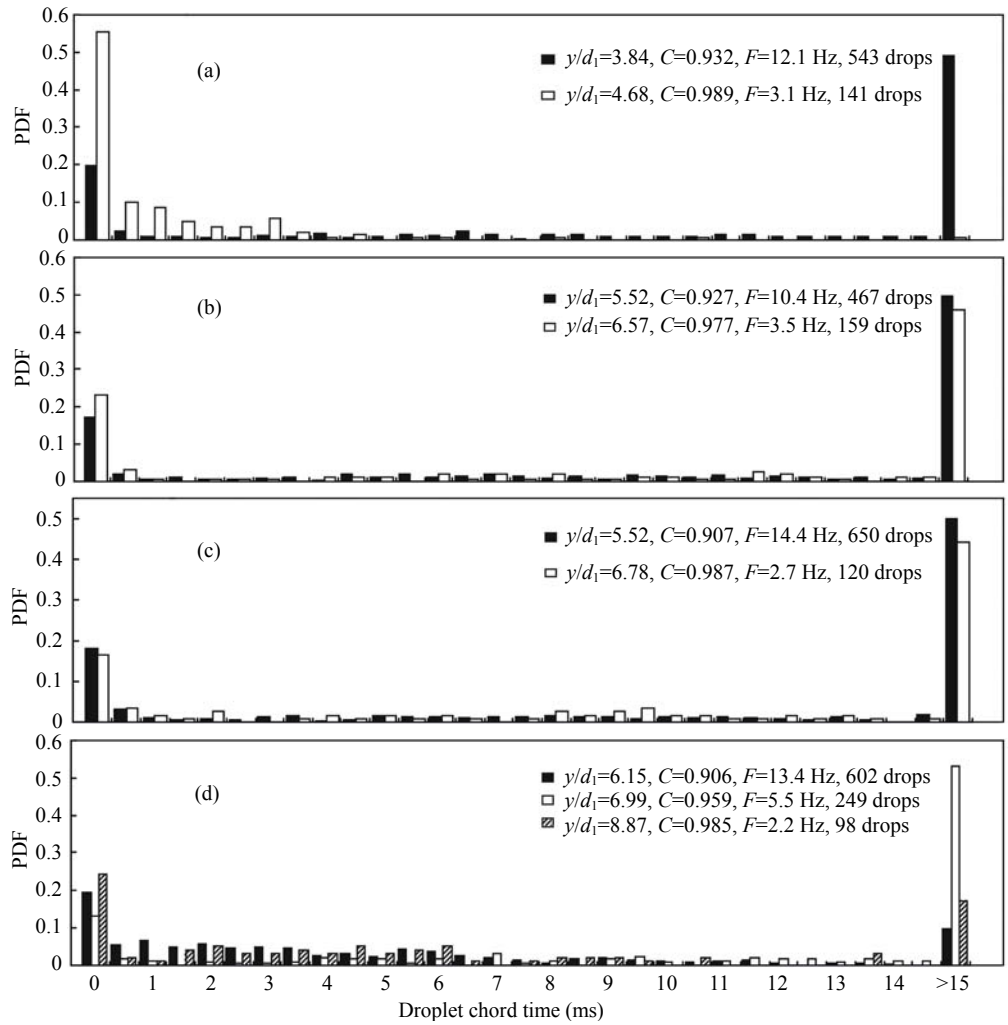

Fig.7 Drop chord time distributions in the spray/mist region, Fr_1=8.5, Re_1=9.8×10^4, d_1=0.025 m, x_1=1.0 m, W=0.50 m. (a) $x-x_1$=0.1 m; (b) $x-x_1$=0.2 m; (c) $x-x_1$=0.3 m; (d) $x-x_1$=0.4 m

In the upper flow region, the void fraction distributions followed a Gaussian error function shape (Eq.(4)). For void fractions larger than 0.70, the flow consisted primarily of water drops and packets surrounded by air: i.e., a spray. Visually significant spray and splashing were noticed above the jump roller. These observations supported the existence of a spray/mist region with small densities of water droplets for C>0.9 and of an upper fog/aerosol region with very-fine water droplets for C>0.99. In these upper spray regions, the distributions of drop chord times did not exhibit a shape similar to the log-normal law. Experimental measurements showed a broad range of ejected drop chord times with flat drop chord time distributions.

It is believed that the present study is the first comprehensive study detailing the two-phase flow properties of both the bubbly and spray regions of hydraulic jumps. It showed the complexity of both zones suggesting that future studies should not be restricted to the bubbly flow region, but encompass the interactions between the bubble entrainment and droplet ejection processes.

ACKNOWLEDGEMENT

The author acknowledges the kind assistance of Mr Graham Illidge.

References

Bakhmeteff, B.A., 1932. Hydraulics of Open Channels, 1st Ed. McGraw-Hill, New York, USA, p.329.

Belanger, J.B., 1840. Essai sur la Solution Numérique de Quelques Problèmes Relatifs au Mouvement Permanent des Eaux Courantes. (Essay on the Numerical Solution of Some Problems Relative to Steady Flow of Water.) Carilian-Goeury, Paris, France (in French).

Brattberg, T., Chanson, H., Toombes, L., 1998. Experimental investigations of free-surface aeration in the developing flow of two-dimensional water jets. *J. Fluids Eng., Trans. ASME*, **120**(4):738-744.

Chanson, H., 1989. Study of air entrainment and aeration devices. *J. Hyd. Res., IAHR*, **27**(3):301-319.

Chanson, H., 1997. Air Bubble Entrainment in Free-Surface Turbulent Shear Flows. Academic Press, London, UK, p.401.

Chanson, H., 1999. Turbulent open-channel flows: drop-generation and self-aeration. *J. Hyd. Engrg., ASCE*, **125**(6):668-670. [doi:10.1061/(ASCE)0733-9429(1999)125:6(668)]

Chanson, H., 2002. Air-water flow measurements with intrusive phase-detection probes. Can we improve their interpretation? *J. Hyd. Engrg., ASCE*, **128**(3):252-255. [doi:10.1061/(ASCE)0733-9429(2002)128:3(252)]

Chanson, H., 2004a. The Hydraulics of Open Channel Flows: An Introduction, 2nd Ed. Butterworth-Heinemann, Oxford, UK, available at http://www.uq.edu.au/~e2hchans/reprints/book3_2.htm

Chanson, H., 2004b. Compressibility of extra-high-velocity aerated flow: a discussion. *J. Hyd. Res., IAHR*, **42**(2):213-215.

Chanson, H., 2006. Air Bubble Entrainment in Hydraulic Jumps: Similitude and Scale Effects. Report No. CH57/05. Dept. Civil Engrg., The University of Queensland, Brisbane, Australia, p.119.

Chanson, H., Brattberg, T., 1998. Air Entrainment by Two-Dimensional Plunging Jets: the Impingement Region and the Very-Near Flow Field. Proc. 1998 ASME Fluids Eng. Conf. Washington DC, USA.

Chanson, H., Brattberg, T., 2000. Experimental study of the air-water shear flow in a hydraulic jump. *International Journal of Multiphase Flow*, **26**(4):583-607. [doi:10.1016/S0301-9322(99)00016-6]

Chanson, H., Gonzalez, C.A., 2004. Interactions between Free-Surface, Free-Stream Turbulence and Cavity Recirculation in Open Channel Flows: Measurements and Turbulence Manipulation. Proc. 5th Intl. Conf. on Multiphase Flow. Paper 104, Yokohama, Japan. p.14 (CD-ROM).

Crowe, C., Sommerfield, M., Tsuji, Y., 1998. Multiphase Flows with Droplets and Particles. CRC Press, Boca Raton, USA, p.471.

Einstein, A., 1906. Eine neue bestimmung der moleküldimensionen. *Ann. Phys.*, **19**:289.

Einstein, A., 1911. Eine neue bestimmung der moleküldimensionen. *Ann. Phys.*, **34**:591.

Henderson, F.M., 1966. Open Channel Flow. MacMillan Company, New York, USA.

Hong, M., Cartellier, A., Hopfinger, E.J., 2004. Characterization of phase detection optical probes for the measurement of the dispersed phase parameters in sprays. *International Journal of Multiphase Flow*, **30**(6):615-648. [doi:10.1016/j.ijmultiphaseflow.2004.04.004]

Hoyt, J.W., Taylor, J.J., 1977. Turbulence structure in a water jet discharging in air. *Physics of Fluids*, **20**(10):253-257. [doi:10.1063/1.861738]

Mossa, M., Tolve, U., 1998. Flow visualization in bubbly two-phase hydraulic jump. *J. Fluids Eng., ASME*, **120**:160-165.

Murzyn, F., Mouaze, D., Chaplin, J.R., 2005. Optical fibre probe measurements of bubbly flow in hydraulic jumps. *International Journal of Multiphase Flow*, **31**(1):141-154. [doi:10.1016/j.ijmultiphaseflow.2004.09.004]

Rajaratnam, N., 1962. An experimental study of air entrainment characteristics of the hydraulic jump. *Journal of the Institution of Engineers, India*, **42**(7):247-273.

Rao, N.S.L., Kobus, H.E., 1971. Characteristics of Self-Aerated Free-Surface Flows. Water and Waste Water/ Current Research and Practice, Vol. 10. Eric Schmidt Verlag, Berlin, Germany.

Rein, M., 1998. Turbulent open-channel flows: drop-generation and self-aeration. *J. Hyd. Engrg., ASCE*, **124**(1):98-102. Discussion, **125**(6):668-670. [doi:10.1061/(ASCE)0733-9429(1998)124:1(98)]

Resch, F.J., Leutheusser, H.J., 1972. Le Ressaut hydraulique: mesure de turbulence dans la région diphasique. (The hydraulic jump: turbulence measurements in the two-phase flow region.) *J. La Houille Blanche*, (4):279-293 (in French).

Thandaveswara, B.S., 1974. Self aerated Flow Characteristics in Developing Zones and in Hydraulic Jumps. Ph.D Thesis, Dept. Civil Engrg., Indian Institute of Science, Bangalore, India, p.399.

Toombes, L., 2002. Experimental Study of Air-Water Flow Properties on Low-Gradient Stepped Cascades. Ph.D Thesis, Dept. Civil Engrg., The University of Queensland.

Wisner, P., 1965. Sur le Rôle du Critère de Froude dans l'Etude de l'Entraînement de l'Air par les Courants à Grande Vitesse. (On the Role of the Froude Criterion for the Study of Air Entrainment in High Velocity Flows.) Proc. 11th IAHR Congress. Paper 1.15, Leningrad, USSR (in French).